Theoretical Chemistry Accounts (2020) 139:164
https://doi.org/10.1007/s00214-020-02681-1

REGULAR ARTICLE

Non-conservation of activation energy barriers in the same chemical process: a cooperative (effect) proton transfer on $(HF)_n$ molecular aggregates

Sara. F. de A. Morais[1,2,3] · **Kleber C. Mundim**[2] · **Daví A. C. Ferreira**[1]

Received: 12 March 2020 / Accepted: 5 October 2020 / Published online: 19 October 2020

Abstract
The formation of $(HF)_n$ aggregates with $n = 2$, 3, 4, 5 and 6 and concerted proton transfer processes in these aggregates were systematically analyzed. It was verified that, by a cooperative effect, the barrier associated with the proton transfer process decreases for aggregates with a larger number of molecules, indicating that the activation energy for proton transfer depends on the molecularity of the process. Natural bond orbital and quantum theory of atoms in molecules were used to characterize the strength of the hydrogen bonds established in the aggregates, which verified a general increase in the delocalization energy as a function of increasing aggregate size. A deformed Eyring (*d*-Eyring) equation was used to calculate the proton transfer rate constants, where the *d*-Eyring equation adequately described the proton transfer kinetics. Analysis of the rate constants showed that proton transfer became faster as the cluster size increased. Arrhenius and *d*-Arrhenius plots showed a decrease in the dependence of the rate constants on temperature, particularly for the tetramer, pentamer, and hexamer. The *d*-Arrhenius plots, for which the *d* parameter was included in the Eyring equation, suggest non-Arrhenius behavior for proton transfer in the HF aggregates at low temperatures.

Keywords Cooperative effects · HF aggregates · Hydrogen bonds · Proton transfer rates

1 Introduction

For several decades, the formation of hydrogen halide aggregates has been explored, driven by the interest in the varied architectures and the nature of the interactions in these aggregates, as well as the resulting properties manifested by molecular cooperativity [1–6]. Among the interactions established between clusters, multicentric interactions (for example, the tricentric bond with three nuclear attractors and two electrons) [7] are usually responsible for the stabilization of a set of atoms in a molecule, and this can be extended to clusters of molecules, and hydrogen bonds, which are special dipole–dipole type interactions involving charge transfer. Systems comprising three nuclear attractors and four electrons may also be formed. These interactions play a fundamental role in self-assembly, conductivity, matter condensation, and various other supramolecular phenomena. Hydrogen bonds (H-bonds) are the main interactive force in the formation of hydrogen halide aggregates, allowing the generation of complex and stable molecular networks that remain cohesive owing to the continuous process of multiple proton exchange, as previously demonstrated theoretically

"Festschrift in honor of Prof. Fernando R. Ornellas" Guest Edited by Adélia Justino Aguiar Aquino, Antonio Gustavo Sampaio de Oliveira Filho and Francisco Bolivar Correto Machado.

Electronic supplementary material The online version of this article (https://doi.org/10.1007/s00214-020-02681-1) contains supplementary material, which is available to authorized users.

✉ Sara. F. de A. Morais
sfam777@gmail.com; saramorais@iq.usp.br

✉ Daví A. C. Ferreira
dacf@unb.br

[1] Laboratório de Dinâmica e Reatividade Molecular, Instituto de Química, Universidade de Brasília, Campus Darcy Ribeiro, CP 04478, Asa Norte - Brasília, DF CEP: 70904-970, Brazil

[2] Laboratório de Modelagem de Sistemas Complexos, Instituto de Química, Universidade de Brasília, Campus Darcy Ribeiro, CP 04478, Asa Norte - Brasília, DF CEP: 70904-970, Brazil

[3] Grupo de Química Computacional Aplicada, Departamento de Química Fundamental, Instituto de Química, Universidade de São Paulo, Av. Prof. Lineu Prestes, 748, São Paulo 05508-000, Brazil

and experimentally for several systems, both in the gas and condensed phases [2–5, 8]. Thus, because the dimensions of aggregates of protonated molecular species are defined as a function of the pressure (concentration) and temperature conditions, the activation energy for the proton transfer processes is expected to vary as a function of the aggregate size, that is, as a function of the molecularity of the proton transfer process [4, 9, 10]. For systems where the products and reagents in the proton transfer process are identical species, such as $(HX)_n$, the change in the rate of proton transfer can be interpreted as a result of tunneling effects because the energy barrier is constant, even for transfers with different molecularities. In this study, we present a systematic theoretical evaluation of the shape, stability, and cohesion of molecular aggregates of type $(HF)_n$ in the gas phase, comparing our observations with experimental and theoretical data, and discuss concerted proton transfer processes based on cooperative effects and non-conservation of the activation energy.

2 Computational details

Geometry optimization and vibrational frequency calculations for all molecular species were performed using the second-order Møller-Plesset perturbation theory (MP2) [11–13] with the def2-QZVP [14, 15] basis set. The Berny [16] algorithm was applied to identify the transition states, and the identity of a transition state was confirmed by the presence of only one imaginary vibrational mode. Quantum theory of atoms in molecules (QTAIM) was used for topological study of the cooperative effects [17, 18]. This analysis provides a more accurate description of the evolution of the electron densities in concerted proton transfer, where cooperative effects are pronounced. Natural bond orbital (NBO) [19–21] analyses were performed to verify the effects of the number of molecules in the cluster on the delocalization energy through established hydrogen bonds and Wiberg bond index (WBI) in NAO (Natural Atomic Orbital) basis of hydrogen bonds was also performed. Gaussian NBO version 3.1 was used for the NBO analysis. Therefore, to calculate the NBO donor–acceptor delocalization energies from second-order perturbation theory, analysis of the Fock matrix in the NBO basis was performed using single point calculations (from the geometries optimized by the MP2 method) using the DFT method by applying the ωB97XD [22] functional and def2-QZVP [14, 15] basis set. Additional geometry calculations of *p*-toluic acid and its dimer were performed with the ωB97XD [22] functional and cc-pVDZ [23, 24] basis set. All calculations presented herein were performed using Gaussian 09 [25] and AIMAll [26] packages. The molecules were visualized using the ChemCraft [27] program.

Finally, to analyze the possibility of describing the proton transfer process as a tunneling effect, the proton transfer rates were determined based on the Eying equation [28] in which the *d*-exponent [10, 29] correction, which includes the Tsallis [30] thermodynamics were employed. The Eyring equation [28] is shown in Eq. 1 and can be written as Eq. 2.

$$k(T) = \frac{k_B T}{h} e^{\left(-\frac{\Delta G^{\ddagger}}{RT}\right)} \tag{1}$$

$$k(T) = \frac{k_B T}{h} e^{\left(\frac{\Delta S^{\ddagger}}{R}\right)} e^{\left(-\frac{E}{RT}\right)} \tag{2}$$

In these equations, k_B is the Boltzmann constant, T is the temperature, h is Planck's constant, R is the universal gas constant, $\Delta G^{\ddagger}$ is the activation Gibbs free energy, $\Delta S^{\ddagger}$ is the activation entropy, and E is the activation energy. The rate constant can also be written as the most common form of the Arrhenius equation [31, 32]:

$$k(T) = Ae^{\left(-\frac{E}{RT}\right)} \tag{3}$$

Thus, using Eq. 2 to calculate the rate constant, the pre-exponential factor, A, is given by:

$$A = \frac{k_B T}{h} e^{\left(\frac{\Delta S^{\ddagger}}{R}\right)} \tag{4}$$

Based on the transition state theory (TST) the activation energy, that will be called E_0 from now on, can be written as the Eq. 5.

$$E_0 = \Delta H^{\ddagger} + \left(1 - \Delta n^{\ddagger}\right) RT \tag{5}$$

In Eq. 5, $\Delta H^{\ddagger}$ is the activation enthalpy and $\Delta n^{\ddagger}$ is the change of molecules number from the reactants to the transition state (TS) formation. For a unimolecular reaction, $\Delta n^{\ddagger} = 0$. Thus, the activation energy for a unimolecular reaction in gas phase is given by Eq. 6.

$$E_0 = \Delta H^{\ddagger} + RT \tag{6}$$

The parameter d was defined as a deformation parameter of the Aquilanti-Mundim [33–35] deformed Arrhenius model (or *d*-Arrhenius) based on the non-extensive entropy formalism of Tsallis [30]. The *d*-exponent is equivalent to $(1-q)$ in the Tsallis formalism [30]. Thus, the rate constant of the *d*-Arrhenius model is given by Eq. 7.

$$k_d(T) = A\left(1 - d\frac{E_0}{RT}\right)^{\frac{1}{d}} \tag{7}$$

The activation barrier E_a can be written as Eq. 6, in which $E_a = E_0$ at the limit $d \to 0$.

$$E_a = -\frac{\partial \ln k_d(T)}{\partial\left(\frac{1}{RT}\right)} = E_0\left(1 - d\frac{E_0}{RT}\right)^{-1} \tag{8}$$

Hence, the activation energy, considering the *d*-Arrhenius model, can be described by Eq. 9.

$$\frac{1}{E_a} = \frac{1}{E_0} - d\left(\frac{1}{RT}\right) \tag{9}$$

The *d*-exponent was correlated for quantum tunneling [29] and the revised parameter *d* is given by Eq. 8. where N_A is Avogadro's constant, ω_i is the TS imaginary vibrational mode, and c is the speed of light.

$$d = -\frac{1}{3}\left(N_A\frac{hc\omega_i}{2E_0}\right)^2 \tag{10}$$

Finally, by further applying the *d*-exponent (Eq. 10), the *d*-Arrhenius model (Eq. 7) in the Eyring's rate constant (Eq. 2) can be rewritten as in Eq. 11, which is called *d*-Eyring's equation.

$$k_d(T) = \frac{k_B T}{h} e^{\left(\frac{\Delta S^{\ddagger}}{R}\right)}\left(1 - d\frac{E_0}{RT}\right)^{\frac{1}{d}} \tag{11}$$

3 Results and discussion

Proton transfer in the HF clusters was evaluated by thermochemical, QTAIM, and NBO analyses of aggregate formation, and by assessing the kinetics of proton transfer in the HF clusters. The optimized ground and transition state (TS) structures of the HF clusters (Fig. 1) were used as the initial reference for the analysis.

The formation of molecular aggregates may be governed by several factors; one of the most important is non-covalent interactions, particularly H-bonds. The nature of these intermolecular forces, i.e., the generation or restriction of new organizational possibilities (microstates), can lead to redistribution of the electronic density of molecular systems and generate new arrangements of molecules. Although the formation of non-covalent interactions such H-bonds is generally followed by electronic stabilization with exothermic characteristics, the molecular arrangements that lead to an entropy decrease must undergo organization. The entropy decrease commonly causes aggregation to be an endergonic process. These processes are initially signaled by observable thermodynamic changes, as highlighted in Table 1.

To verify the accuracy of our thermochemical data for HF cluster formation, we compared the calculated enthalpies obtained in this work (Table 1) with the experimental enthalpies for HF aggregation reported by Redington [36]. The deviation was below 2.0 kcal/mol, which is considered acceptable. Analysis of the relative free energy of aggregate formation indicated that aggregate formation was endergonic, with the exception of the pentamer,

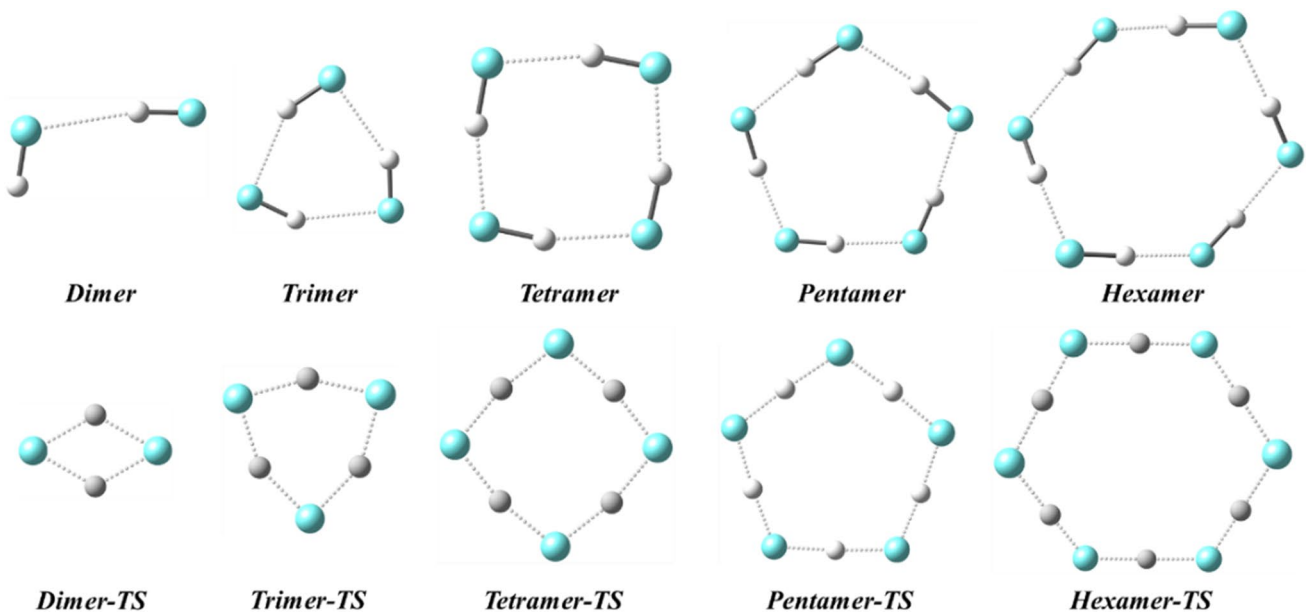

Fig. 1 Molecular architectures of HF aggregates: dimer, trimer, tetramer, pentamer, and hexamer (with respective TS geometries)

Table 1 Thermochemical data for formation of HF aggregates

Aggregates	ΔH_{exp}	ΔH	ΔG	ΔS	ΔS_{vib}
HF	–	0.00	0.00	0.00	0.00
Dimer	−2.27	−3.62	2.45	−20.37	5.76
Trimer	−11.28	−12.52	3.23	−52.81	8.61
Tetramer	−23.19	−24.08	0.80	−83.43	16.72
Pentamer	−31.57	−33.32	−0.74	−109.27	29.98
Hexamer	−39.39	−41.36	1.15	−142.59	36.21

The Gibbs free energies (ΔG) and enthalpies (ΔH) are in kcal/mol and the entropies (ΔS) and vibrational entropies (ΔS_{vib}) are in cal/mol K. The properties are relative to those of the HF monomer. The experimental enthalpies (ΔH_{exp}) for HF aggregation were obtained from the work of Redington [36]

which exhibited exergonic behavior. Although, aggregate formation became more exothermic with an increase in the aggregate size, the decrease in the entropy due to the increase (in relation to the monomer) in the number of molecules in the aggregate makes aggregation endergonic for all clusters, except for the pentamer. Thus, aggregate formation is directly dependent on entropic factors (Table 1).

Thermodynamic analysis of proton transfer in the HF aggregates (Table 2) showed that proton transfer is more favorable in larger aggregates. The activation energy for proton transfer decreased with an increase in the HF cluster size. Although pentamer formation is more favorable than formation of the hexamer (and all other clusters), proton transfer in the pentamer required a higher activation Gibbs energy than in the hexamer. However, the hexamer-TS has a higher activation energy (E_0) than the pentamer-TS. Again, entropy plays an important role in the reactivity of these systems. The arrangement of the hexamer in the proton transfer TS allows for a smaller entropy decrease than in the pentamer (a positive change in the activation entropy of the hexamer in relation to the pentamer) favoring proton transfer at high temperatures. This behavior is reflected in the rate constant of proton transfer, which is higher for the hexamer than for the pentamer, as will be discussed.

Although aggregation led to a decrease in the entropy, the entropic vibrational contribution increased for larger clusters. This behavior indicates that the cooperative effects are enthalpically directed and have a positive contribution to entropic vibrational components. Thus, thermodynamic analysis of proton transfer in the HF aggregates demonstrated that the proton transfer process is facilitated by cooperative effects with increasing aggregate size. In addition, pentamer formation proved to be a spontaneous process.

NBO analysis of the molecular orbitals was used to probe the level of cooperativity in the molecular networks formed by the HF aggregates. The representations of the donor–acceptor ($n_F \rightarrow \sigma^*_{H-F}$) NBO interaction in the HF clusters for a hydrogen bond are shown in Fig. 2. The representations of the remaining NBOs for the donor–acceptor interactions of hydrogen bonds in the HF clusters are presented in the Supplementary Material. The NBO delocalization energies and WBI are listed in Table 3.

The present analysis indicates that the delocalization energy of the donor–acceptor interaction $n_F \rightarrow \sigma^*_{H-F}$ increases with an increase in the number of molecules in the aggregate. Along with these results the WBI indicates a strengthening of H-bonds with the increase of molecules in the HF aggregates. Although the delocalization energy of the donor–acceptor interaction increased, as the strengthening of H-bonds, for larger clusters, this increase was not additive. These observations are due to a set of structural factors that favor the orbital symmetry number involved in the formation of hydrogen bonds in the network and, consequently, better interactions between molecules in the aggregate. The selected geometrical parameters of the hydrogen bonds in HF clusters that support this observation are shown in Table 4. The analysis of bond lengths and angles of H-bonds demonstrates that there is a decrease of H-bond length accompanied by an increase of F–H bond length when the number of molecules in the cluster increase; this behavior agrees with the trends verified by NBO analysis. Besides that, the bond angles

Table 2 Thermochemical data, imaginary vibrational mode of TS and parameter d for proton transfer in HF aggregates

Aggregates-TS	$\Delta H^{\neq}$	$\Delta G^{\neq}$	$\Delta S^{\neq}$	$\Delta S^{\neq}_{vib}$	E_a	ω_i	d
Dimer-TS	37.15	39.98	−9.49	−5.49	37.77	−225,054.44	-2.42×10^{-3}
Trimer-TS	14.46	16.84	−7.99	−7.10	15.06	−172,279.05	-8.90×10^{-3}
Tetramer-TS	6.99	9.62	−8.82	−8.19	7.58	−147,844.66	-2.58×10^{-2}
Pentamer-TS	5.39	8.48	−10.37	−9.82	5.99	−140,894.37	-3.77×10^{-2}
Hexamer-TS	6.35	7.38	−3.43	−2.86	6.95	−139,758.72	-2.75×10^{-2}

The activation Gibbs free energies ($\Delta G^{\neq}$) and activation enthalpies ($\Delta H^{\neq}$) are in kcal/mol and the activation entropies ($\Delta S^{\neq}$) and activation vibrational entropies ($\Delta S^{\neq}_{vib}$) are in cal/mol.K. The properties are relative to the respective ground-state HF aggregates. The activation energy (E_0) was calculated through the Eq. 6 with $T = 298.15$ K. Further, ω_i (in m^{-1}) is the imaginary vibrational mode of the TS. The parameter d was calculated by applying the Eq. 10

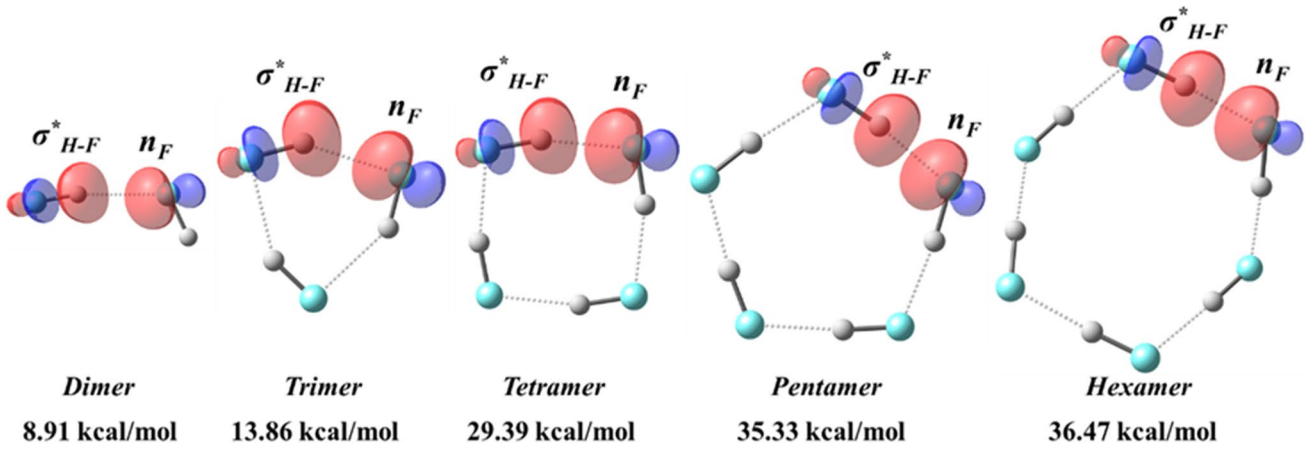

Fig. 2 Natural molecular orbitals involved in hydrogen bonds in HF aggregates with respective delocalization energies

Table 3 NBO delocalization energies ($E^{(2)}$) of donor–acceptor interactions and Wiberg bond index (WBI) in NAO basis for hydrogen bonds (H···F) in HF aggregates

HF aggregates	donor	acceptor	$E^{(2)}$ (kcal/mol)	WBI
Dimer	n_F	σ^*_{H-F}	8.91	0.0002
Trimer	n_F	σ^*_{H-F}	13.86	0.0416
Tetramer	n_F	σ^*_{H-F}	29.39	0.0798
Pentamer	n_F	σ^*_{H-F}	35.33	0.0929
Hexamer	n_F	σ^*_{H-F}	36.47	0.0953

Table 4 Geometrical parameters and for hydrogen bond in HF aggregates

HF aggregates	Bond lengths (Å)	Bond angles (°)	
	F–H	H···F	F–H···F
Dimer	0.923	1.821	170.09
Trimer	0.935	1.759	147.23
Tetramer	0.947	1.588	164.71
Hexamer	0.947	1.536	173.97
Pentamer	0.952	1.524	177.18

of H-bond interaction have a similar trend, however due to the ring tension the trimer and tetramer have their F–H···F angle smaller than others. A point to note is that there is a greater difference between the H-bond lengths for the HF dimer, trimer, and tetramer than between the H-bonds lengths for the HF tetramer, pentamer, and hexamer. This trend was also observed for the differences between delocalization energies ($E^{(2)}$) among HF clusters and also in the thermochemical analysis of H-bonds in HF aggregates formation. This behavior demonstrate that the cooperative effects involved in H-bonds of HF aggregates formation have a non-additive characteristic which resides in several factors and the structural arrangement is one of the main limiting for it.

QTAIM analysis was used for topological verification of the electron density redistribution in the HF aggregates. This analysis may provide information on the relative variation in the hydrogen bonding domains as a function of the aggregate size. The attractors and bond critical points (BCP) connected through bond paths (BP) are graphically represented in Fig. 3, and the AIM properties are listed in Table 5.

QTAIM analysis of the ground-state HF clusters demonstrates a strengthening of the H···F hydrogen bonds (BCP ***b***) as the number of HF molecules in the aggregate increases, which consequently weakens the H–F bonds (BCP ***a***). This can be verified by the increase in the electronic density (ρ) at BCP ***b***, which relates to the hydrogen bonds, and a decrease in ρ at BCP ***a***, which is related to the H–F bond. Besides that, the positive values of the Laplacian density ($\nabla^2\rho$) for the H-bonds (BCP ***b***) indicate that they are non-covalent interactions. Furthermore, the increase of the absolute value of electronic potential energy density (V) at the BCP ***b*** demonstrate the increase of electrons stability in the H-bonds as the number of HF molecules in the clusters increase. In contrast, the H–F bonds showed negative values of $\nabla^2\rho$ demonstrating that H–F are covalent bonds. However, the decrease of absolute values of $\nabla^2\rho$ and V along with the increase of magnitude of the ellipticity (ε) at BCP ***a*** (indicating redistribution of the electron density in the H–F bond) demonstrating the weakening of the H–F bond as the number of molecules in the clusters increase. Finally, the AIM analysis proving that the H-bonds in HF aggregates became stronger as the size of the HF aggregate increases through cooperative effects and this strengthening is non-additive as verified previously by thermochemical and NBO analysis. This behavior was also observed for the proton transfer transition states in the HF aggregates in which the H···F bonds in the TS became stronger as the number of HF molecules

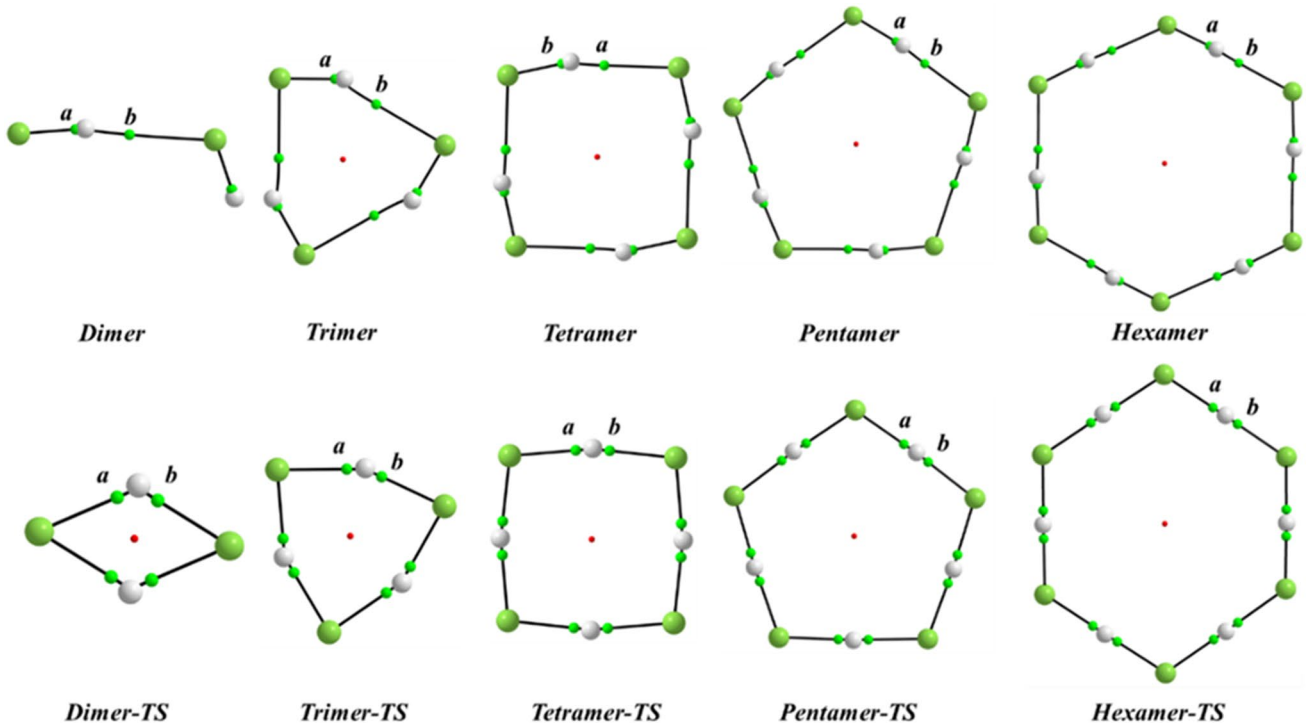

Fig. 3 QTAIM representation of the BCPs and BPs in the $(HF)_n$ aggregates with different HF molecularities ($n=2$, 3, 4, 5, and 6) and the respective proton transfer transition states (TS). The small green spheres are the bond critical points (BCPs), the black lines between attractors (F and H atoms) are the bond paths (BPs), and the small red spheres are the ring critical point (RCP)

Table 5 AIM properties of highlighted BCPs ***a*** and ***b*** for HF aggregates and the respective TSs shown in Fig. 3

	a				***b***			
	ρ	$\nabla^2\rho$	ε	V	ρ	$\nabla^2\rho$	ε	V
Monomer	0.3781	−3.8994	0.0000	−1.1812	–	–	–	–
Dimer	0.3681	−3.9371	0.0001	−1.1839	0.0256	+0.1033	0.0275	−0.0254
Trimer	0.3504	−3.7836	0.0004	−1.1316	0.0329	+0.1190	0.0463	−0.0348
Tetramer	0.3330	−3.5606	0.0008	−1.0752	0.0496	+0.1382	0.0091	−0.0610
Pentamer	0.3262	−3.4689	0.0011	−1.0526	0.0558	+0.1423	0.0194	−0.0721
Hexamer	0.3247	−3.4587	0.0012	−1.0499	0.0570	+0.1437	0.0211	−0.0745
Dimer-TS	0.1657	−0.3993	0.1596	−0.3201	0.1657	−0.3993	0.1596	−0.3201
Trimer-TS	0.1745	−0.5681	0.0166	−0.3589	0.1745	−0.5681	0.0166	−0.3589
Tetramer-TS	0.1781	−0.6226	0.0021	−0.3798	0.1781	−0.6226	0.0021	−0.3798
Pentamer-TS	0.1791	−0.6421	0.0066	−0.3877	0.1791	−0.6421	0.0066	−0.3877
Hexamer-TS	0.1795	−0.6476	0.0067	−0.3903	0.1795	−0.6476	0.0067	−0.3903

Electronic densities (ρ), Laplacian of the electronic density ($\nabla^2\rho$), bond ellipticity (ε), and density of potential energy (V). All quantities measured in atomic units (a.u.)

in the cluster increased, as verified by the AIM properties of BCPs ***a*** and ***b*** for the TS in Table 5. The ρ, $\nabla^2\rho$, ε, and V values were the same for BCP ***a*** and ***b***, as expected for a proton transfer TS. The strengthening of the H···F bonds in the proton transfer TS as the HF molecularity in the cluster increases demonstrates that the influence of the cooperative effects in the electronic structure of the bonds involved in the proton transfer, facilitating the transfer process.

According to Loerting [4] and coworkers, the expected rate of proton transfer in the HF pentamer at 300 K is $k=2.86\times10^9$ s^{-1}, where the comparison was made against the experimental rate of proton transfer for carboxylic acids under the same thermal conditions. Thus, to verify the accuracy of the developed kinetic model, the rate constant for proton transfer in *p*-toluic acid dimers was calculated for comparison with the experimental data obtained by Ernst

[37] and coworkers; this value was used as a reference by Loerting [4]. Ernst [37] and coworkers achieved an E_0 of 1.15 kcal/mol, a rate constant k of 2.0×10^{10} s^{-1} at 300 K, and a pre-exponential factor $A=1.0\times10^{11}$ s^{-1} for proton transfer in the *p*-toluic acid dimer. We then performed calculations for proton transfer in the *p*-toluic acid dimer (*p*-ta-d) with the ωB97XD/cc-pVDZ method. The theoretical rate constant for proton transfer was calculated by applying two different equations: the Eyring equation [28] (Eq. 2) and the *d*-Eyring equation (Eq. 11), in which a correction for hypothetical quantum tunneling in the proton transfer processes is made by including the *d*-exponent. The calculated rate constants and pre-exponential factors are listed in Table 6. The other thermochemical data for proton transfer in the *p*-toluic acid dimer are shown in Table S2.

The activation energy for proton transfer in the *p*-toluic acid dimer achieved in this work was closer to that observed by Ernst [37] and coworkers (with a difference of 0.5 kcal/mol), and the pre-exponential factor was also closer (of the same order of magnitude). Furthermore, the rate constant calculated by applying the Eyring equation (Eq. 2) (k) was very close to the experimentally observed value reported by Ernst [37] and coworkers (2.0×10^{10} s^{-1}). The rate constant k_d (calculated by applying the *d*-Eyring equation (Eq. 11)) was also of the same order of magnitude as the experimental rate constants. Thus, we considered the developed model suitable for calculating the rate constants for proton transfer in HF clusters.

The kinetics of proton transfer in the HF clusters was analyzed by applying two different kinetics models in which the rate constants were, respectively, calculated by applying the Eyring equation (Eq. 2) (k) and the *d*-Eyring equation (Eq. 11) (k_d). The pre-exponential factors and the calculated rate constants (at 300 K) are summarized in Table 7, and the Arrhenius and *d*-Arrhenius plots (ln k vs. $1/T$) are shown in Fig. 4. The data used to calculate the rate constants ($\Delta H^{\ddagger}$, $\Delta S^{\ddagger}$, E_0 for both equations and ω_i, and parameter d for *d*-Eyring (Eq. 11)) are listed in Table 2.

It was verified that proton transfer in the HF aggregates occurred similarly and rapidly in arrangements involving tetramers, pentamers, and hexamers (Fig. 4). For these three clusters, the effect of temperature on the change in the transfer speed is small, particularly at high temperatures. However, the temperature starts to play a significant role in the proton transfer rates at low temperatures, particularly for the pentamers and hexamers. The rate trend is inverted for the pentamer and hexamer at low temperatures so that the proton transfer becomes faster in the pentamer than in the hexamer below 138 K for k and below 128 K for k_d. In order to clarify this behavior, we separated the Arrhenius and the *d*-Arrhenius plots in two plots (one at high temperatures, in the 1000–140 K range for k and 11,000–30 K for k_d and the other at low temperatures, in the 138–2 K range for k and 128–2 K for k_d) as shown in Fig. 5 (for high temperatures) and Fig. 6 (for low temperatures). At high temperatures, the *d*-Arrhenius plot (Fig. 5, right) became very close to the expected behavior for an Arrhenius plot (Fig. 5, left). However, it was verified that for the pentamer (which has a smaller E_0 than the hexamer but for which the change in the activation entropy is more negative than for the hexamer), the rate constant was positively affected by decreasing the temperature in relation to that of the hexamer.

Thus, to evaluate the contributions of the pre-exponential and exponential factors to the rate constant, the values were calculated separately; the results are presented in Table 8. The rate factors (as rate constants) were calculated by applying the *d*-Eyring equation (Eq. 11) for the pentamer and hexamer at 300 K and 100 K. Analyzing the decomposition of the rate constant (as the rate factors) verified that the pentamer has a smaller pre-exponential and higher exponential factor than the hexamer, for both temperatures (100 K and 300 K). However, the temperature affects the magnitude of the difference between these factors and changes the rate constant. The difference between the pre-exponential values for the pentamer and hexamer decreases and that between

Table 7 Proton transfer pre-exponential factors (A) and rate constants (k) calculated by applying Eyring's equation (Eq. 2) (k) and *d*-Eyring's equation (Eq. 11) (k_d) with different molecularities ($n=2$, 3, …, 6) and at 300 K

HF molecularities	A	k	k_d
Dimer	5.26×10^{10} s^{-1}	1.55×10^{-17} s^{-1}	1.27×10^{-15} s^{-1}
Trimer	1.12×10^{11} s^{-1}	1.17 s^{-1}	13.99 s^{-1}
Tetramer	7.36×10^{10} s^{-1}	2.17×10^{5} s^{-1}	1.22×10^{6} s^{-1}
Pentamer	3.37×10^{10} s^{-1}	1.46×10^{6} s^{-1}	6.71×10^{6} s^{-1}
Hexamer	1.11×10^{12} s^{-1}	9.57×10^{6} s^{-1}	4.51×10^{7} s^{-1}

Table 6 Thermochemical data, pre-exponential factors (A), parameter d and rate constants (k) for proton transfer in *p*-toluic acid dimer (*p*-ta-d)

	$\Delta G^{\neq}$	$\Delta S^{\neq}$	E_0	d	A	k	k_d
p-ta-d -TS	2.58	−5.10	1.65	−0.3513	4.79×10^{11} s^{-1}	2.98×10^{10} s^{-1}	6.90×10^{10} s^{-1}

The activation Gibbs free energy ($\Delta G^{\neq}$) and the activation energy (E_0) are in kcal/mol and the activation entropy is in cal/mol.K. The activation energy E_0 was calculated through the Eq. 6 with $T=298.15$ K and parameter d was calculated by the Eq. 10. The rate constants (k and k_d) were calculated by applying two different equations: the Eyring equation (Eq. 2) (k) and the *d*-Eyring equation (Eq. 11) (k_d), both at 300 K

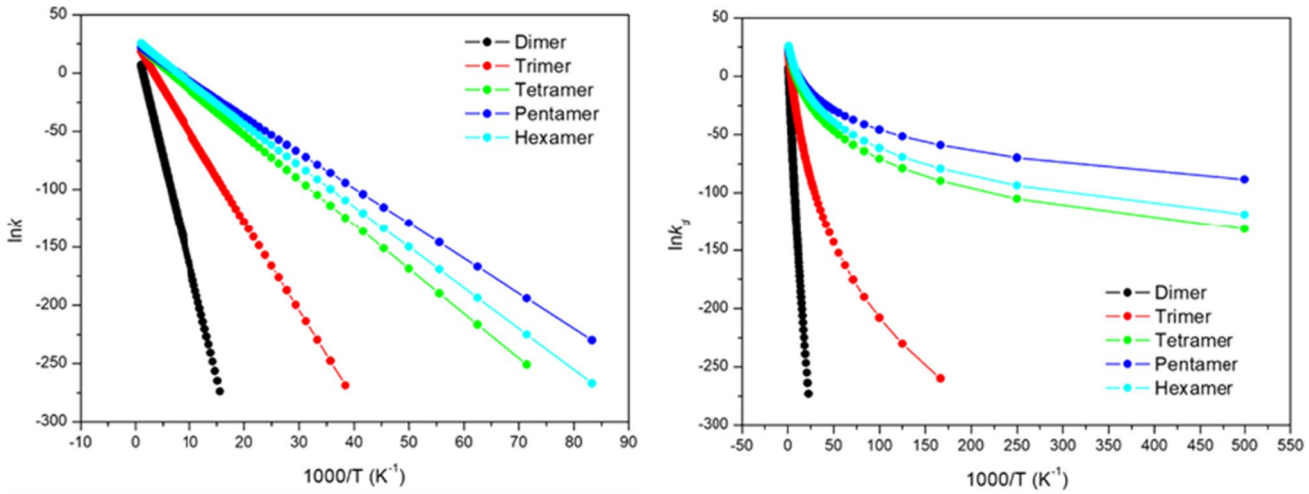

Fig. 4 Arrhenius plot (left) and *d*-Arrhenius plot (right) for rate constants of proton transfer in HF aggregates, calculated using Eyring equation (Eq. 2) and *d*-Eyring equation (Eq. 11), respectively, at 1000–2 K

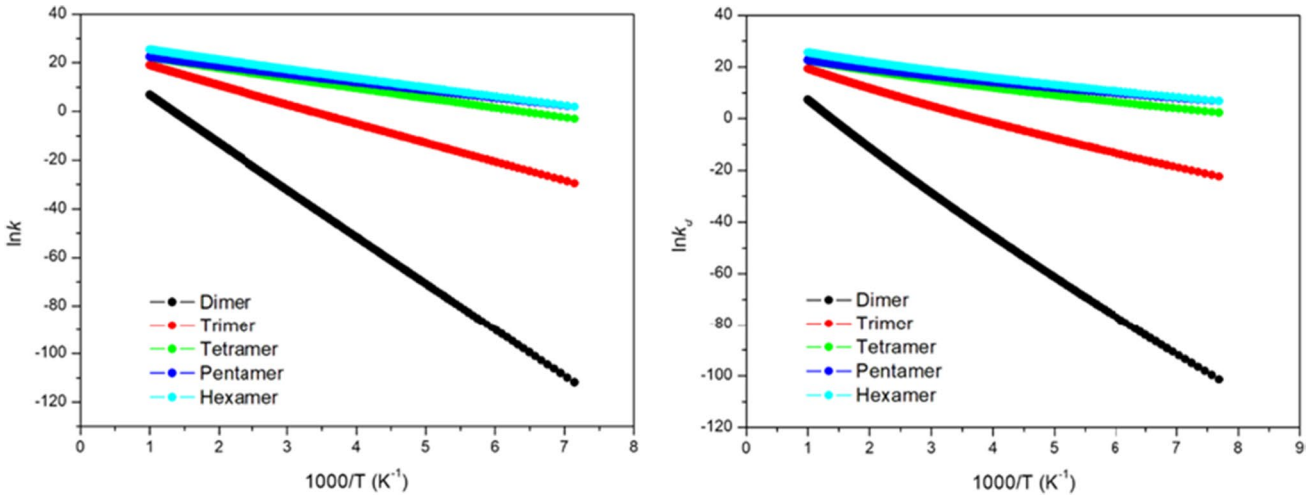

Fig. 5 Arrhenius plot (left) and *d*-Arrhenius plot (right) for rate constants of proton transfer in HF aggregates, calculated using Eyring equation (Eq. 2) at 1000–140 K and *d*-Eyring equation (Eq. 11) at 1000–130 K, respectively

their exponential factors increases at low temperatures. That is, at low temperatures, the exponential factor of the rate constant (which includes E_0) becomes more important, while the entropy (included in the pre-exponential factor) has slightly less influence on the rate constant. Thus, proton transfer becomes faster in the pentamer than in the hexamer below 130 K. This behavior was also verified for the rate constants calculated using the Eyring equation (Eq. 2).

Therefore, although the results obtained with the classical Eyring equation were closer to the experimental data at 300 K than those obtained with the *d*-Eyring equation, the developed model is highlighted because it seeks to include neglected effects, such as the possibility of quantum effects and the influence of the vibration mode on the transition state (ω_i) by including the *d*-exponent in Eyring's [28] equation (Eq. 2). One of the most important effect occur in the activation barrier E_a from the d-Arrhenius model (given by the Eq. 8) which has a great dependency on low temperatures while the activation energy E_0 has a slightly dependency on temperature being almost constant as can be verified in the E_a versus T and E_0 versus T plots in Fig. 7. The activation barrier Ea considerably decreases by low temperatures as function of these effects. This non-Arrhenius behavior is not predicted by the classical Eyring equation and may be important in studies of HF aggregates at low temperatures.

The study shows that the inclusion of such effects does not have great influence at high temperatures, but at low temperatures, causes a curvature in the *d*-Arrhenius plots, and

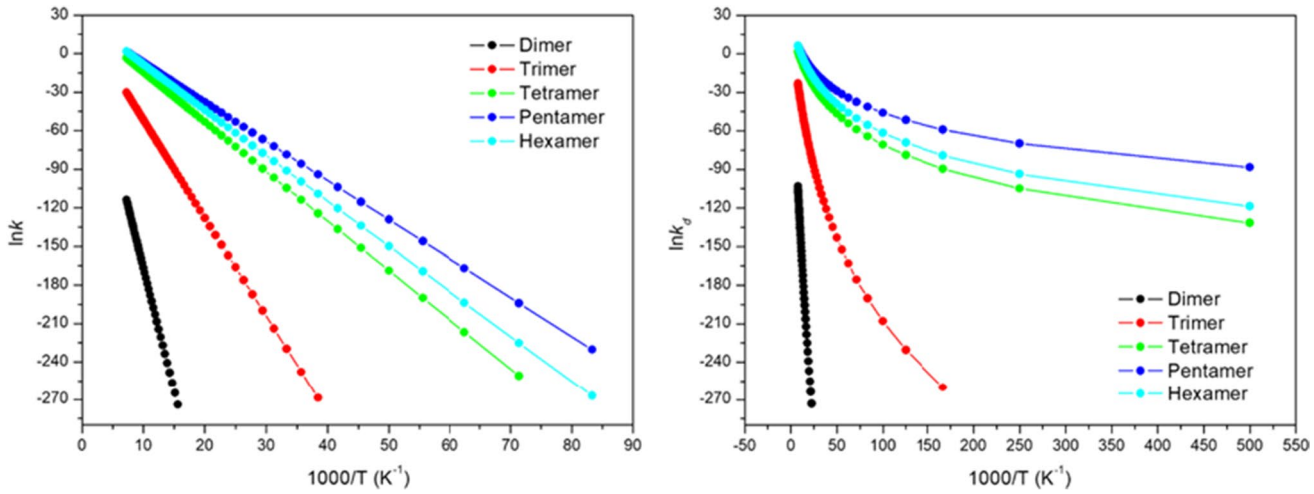

Fig. 6 Arrhenius plot (left) and *d*-Arrhenius plot (right) for rate constants of proton transfer in HF aggregates, calculated using Eyring equation (Eq. 2) at 138–2 K and *d*-Eyring's equation (Eq. 11) at 128–2 K, respectively

Table 8 Activation energy, rate constant (k_d) of proton transfer in *p*-toluic acid dimer, and pre-exponential factor at 300 K

Temperature	Rate factors	Pentamer	Hexamer
300 K	Pre-exponential factor	3.37×10^{10} s^{-1}	1.11×10^{12} s^{-1}
	Exponential factor	1.99×10^{-4}	4.06×10^{-5}
	Rate (k_d)	6.71×10^{6} s^{-1}	4.51×10^{7} s^{-1}
100 K	Pre-exponential factor	1.12×10^{10} s^{-1}	3.71×10^{11} s^{-1}
	Exponential factor	1.80×10^{-9}	2.29×10^{-11}
	Rate (k_d)	20.17 s^{-1}	8.50 s^{-1}

also demonstrates that proton transfer in the HF tetramer, pentamer, and hexamer has less influence on the rate constants at low temperatures, which is not apparent in the classical Arrhenius plots. The cooperative effects presented in HF aggregates formation showed also important to facilitate the proton transfer in HF clusters. These such effects acted as kind of a catalyst behavior generating a new reaction path with lower activation barrier for the same chemical process through a new molecule's arrangement. This behavior can be important to the study of reactions mechanisms which can have their molecules arrangement changed by non-covalent

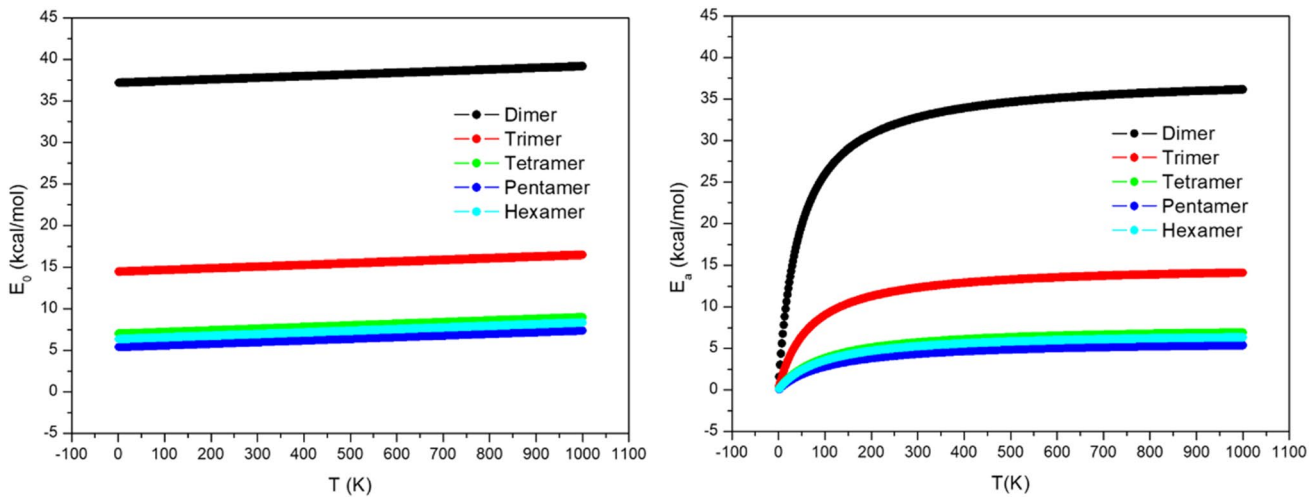

Fig. 7 Activation energy (E_0) versus Temperature (T) plot (left) and activation barrier (E_a) versus Temperature (T) plot (right) for proton transfer in HF aggregates. Temperatures between 2 K-1000 K. E_0 was calculated through Eq. 6 and E_a was calculated through Eq. 8

interactions as H-bonds and through cooperative effects create alternative reaction paths with lower activation energy.

4 Conclusions

Even though the formation of aggregates is, a priori, endergonic, it can be enthalpically directed and, in entropic terms, favored by the entropic vibrational contribution, leading to the formation of thermochemically more stable aggregates. From the topological point of view, increasing the number of HF molecules in the aggregate is accompanied by strengthening of the H···F hydrogen bond, which, in turn, becomes stronger as the size of the aggregate increases. It was found that larger aggregates undergo faster proton transfer in HF aggregates. Our kinetic analysis corroborates the idea that the effects of molecular changes are more likely to be responsible for ultra-fast reaction phenomena. The study demonstrate that cooperative effects can generate new reaction paths with lower activation energy for the same chemical process proving it can be particularly important in mechanism studies of reactions that involve proton transfers and molecules that can stablish non-covalent interactions.

Acknowledgments The authors acknowledge grants from the following Brazilian Institutions: CAPES, CNPQ, and UnB.

References

1. Atoji M, Lipscomb WN (1954) The crystal structure of hydrogen fluoride. Acta Crystallogr 7:173–175
2. Hunt SW, Higgins KJ, Craddock MB et al (2003) Influence of a polar near-neighbor on incipient proton transfer in a strongly hydrogen bonded complex. J Am Chem Soc 125:13850–13860. https://doi.org/10.1021/ja030435x
3. Kuśmierczuk W, Witkowski A (1981) Infrared spectra of hydrogen-bonded hydrogen halides. Chem Phys Lett 81:558–559. https://doi.org/10.1016/0009-2614(81)80462-9
4. Loerting T, Liedl KR, Rode BM (1998) Large curvature tunneling effects reveal concerted hydrogen exchange rates in cyclic hydrogen fluoride clusters comparable to carboxylic acid dimers. J Am Chem Soc 120:404–412. https://doi.org/10.1021/ja972799t
5. Quack M, Schmitt U, Suhm MA (1997) FTIR spectroscopy of hydrogen fluoride clusters in synchronously pulsed supersonic jets Isotopic isolation, substitution and 3-d condensation. Chem Phys Lett 269:29–38. https://doi.org/10.1016/S0009-2614(97)00203-0
6. Roohi H, Taghezadeh R (2011) Intra-cluster proton transfer in anilide–(HF)n (n = 1–4): Can the size of HF cluster influence the N − ···H–F → N–H···F − switching. J Fluor Chem 132:459–467. https://doi.org/10.1016/j.jfluchem.2011.04.018
7. de Giambiagi MS, de Neto MO, de Neder AVF (2005) Cooperative effect of CH···O bonds in models for biological systems. J Math Chem 38:519–532. https://doi.org/10.1007/s10910-005-6905-3
8. Io A, Kawatsu T, Tachikawa M (2019) Quantum stabilization of the frustrated hydrogen bonding structure in the hydrogen fluoride trimer. J Phys Chem A 123:7950–7955. https://doi.org/10.1021/acs.jpca.9b04407
9. Quack M, Schmitt U, Suhm MA (1993) Evidence for the (HF) 5 complex in the HF stretching FTIR absorption spectra of pulsed and continuous supersonic jet expansions of hydrogen fluoride. Chem Phys Lett 208:446–452. https://doi.org/10.1016/0009-2614(93)87171-X
10. Morais SF de A, Mundim KC, Ferreira DAC (2015) An alternative interpretation of the ultracold methylhydroxycarbene rearrangement mechanism: cooperative effects. Phys Chem Chem Phys 17:7443–7448. https://doi.org/10.1039/C4CP05842A
11. Frisch MJ, Head-Gordon M, Pople JA (1990) A direct MP2 gradient method. Chem Phys Lett 166:275–280. https://doi.org/10.1016/0009-2614(90)80029-D
12. Frisch MJ, Head-Gordon M, Pople JA (1990) Semi-direct algorithms for the MP2 energy and gradient. Chem Phys Lett 166:281–289. https://doi.org/10.1016/0009-2614(90)80030-H
13. Head-Gordon M, Head-Gordon T (1994) Analytic MP2 frequencies without fifth-order storage. Theory and application to bifurcated hydrogen bonds in the water hexamer. Chem Phys Lett 220:122–128. https://doi.org/10.1016/0009-2614(94)00116-2
14. Weigend F (2006) Accurate Coulomb-fitting basis sets for H to Rn. Phys Chem Chem Phys 8:1057–1065. https://doi.org/10.1039/B515623H
15. Weigend F, Ahlrichs R (2005) Balanced basis sets of split valence, triple zeta valence and quadruple zeta valence quality for H to Rn: Design and assessment of accuracy. Phys Chem Chem Phys 7:3297–3305. https://doi.org/10.1039/B508541A
16. Schlegel HB (1982) Optimization of equilibrium geometries and transition structures. J Comput Chem 3:214–218. https://doi.org/10.1002/jcc.540030212
17. Bader RFW (1991) A quantum theory of molecular structure and its applications. Chem Rev 91:893–928. https://doi.org/10.1021/cr00005a013
18. Bader RFW (1994) Atoms in molecules: a quantum theory. Clarendon Press, Oxford
19. Reed AE, Curtiss LA, Weinhold F (1988) Intermolecular interactions from a natural bond orbital, donor-acceptor viewpoint. Chem Rev 88:899–926. https://doi.org/10.1021/cr00088a005
20. Reed AE, Weinhold F (1985) Natural localized molecular orbitals. J Chem Phys 83:1736–1740. https://doi.org/10.1063/1.449360
21. Reed AE, Weinstock RB, Weinhold F (1985) Natural population analysis. J Chem Phys 83:735–746. https://doi.org/10.1063/1.449486
22. Chai J-D, Head-Gordon M (2008) Long-range corrected hybrid density functionals with damped atom–atom dispersion corrections. Phys Chem Chem Phys 10:6615–6620. https://doi.org/10.1039/B810189B
23. Dunning TH (1989) Gaussian basis sets for use in correlated molecular calculations. I. The atoms boron through neon and hydrogen. J Chem Phys 90:1007–1023. https://doi.org/10.1063/1.456153
24. Kendall RA, Dunning TH, Harrison RJ (1992) Electron affinities of the first-row atoms revisited. Systematic basis sets and wave functions. J Chem Phys 96:6796–6806. https://doi.org/10.1063/1.462569
25. Frisch MJ, Trucks GW, Schlegel HB et al (2009) Gaussian 09, Revision B.01. Gaussian 09, Revis. B.01, Gaussian, Inc., Wallingford CT
26. Keith TA (2017) AIMAll (Version 16.05.18)
27. Andrienko GA (2015) Chemcraft—graphical software for visualization of quantum chemistry computations. https://www.chemcraftprog.com
28. Eyring H (1935) The activated complex and the absolute rate of chemical reactions. Chem Rev 17:65–77. https://doi.org/10.1021/cr60056a006
29. Silva VHC, Aquilanti V, de Oliveira HCB, Mundim KC (2013) Uniform description of non-Arrhenius temperature dependence

of reaction rates, and a heuristic criterion for quantum tunneling vs classical non-extensive distribution. Chem Phys Lett 590:201–207. https://doi.org/10.1016/j.cplett.2013.10.051
30. Tsallis C (1988) Possible generalization of Boltzmann–Gibbs statistics. J Stat Phys 52:479–487. https://doi.org/10.1007/BF01016429
31. Arrhenius S (1889) Über die Reaktionsgeschwindigkeit bei der Inversion von Rohrzucker durch Säuren. Zeitschrift für Phys Chemie 4U:226–248. https://doi.org/10.1515/zpch-1889-0416
32. Mulyava MT, Shevchuk VU (1967) Calculation of pre-exponential factors for radical substitution reactions on the basis of the additivity principle. Theor Exp Chem 1:482–485. https://doi.org/10.1007/BF00524032
33. Aquilanti V, Mundim KC, Elango M et al (2010) Temperature dependence of chemical and biophysical rate processes: phenomenological approach to deviations from Arrhenius law. Chem Phys Lett 498:209–213. https://doi.org/10.1016/j.cplett.2010.08.035
34. Aquilanti V, Borges EP, Coutinho ND et al (2018) From statistical thermodynamics to molecular kinetics: the change, the chance and the choice. Rend Lincei Sci Fis e Nat 29:787–802. https://doi.org/10.1007/s12210-018-0749-9
35. Contributors W Aquilanti–Mundim deformed Arrhenius model. In: Wikipedia, Free Encycl
36. Redington RL (1982) Nonideal-associated vapor analysis of hydrogen fluoride. J Phys Chem 86:552–560. https://doi.org/10.1021/j100393a027
37. Meier BH, Graf F, Ernst RR (1982) Structure and dynamics of intramolecular hydrogen bonds in carboxylic acid dimers: a solid state NMR study. J Chem Phys 76:767–774. https://doi.org/10.1063/1.443045